Official journal of the CIOMP 2047-7538
www.nature.com/lsa

ARTICLE Open Access

Bright semiconductor single-photon sources pumped by heterogeneously integrated micropillar lasers with electrical injections

Xueshi Li[1], Shunfa Liu[1], Yuming Wei[1], Jiantao Ma[1], Changkun Song[1], Ying Yu[1], Rongbin Su[1], Wei Geng[2], Haiqiao Ni[3,4], Hanqing Liu[3,4], Xiangbin Su[3,4], Zhichuan Niu[3,4]✉, You-ling Chen[3,4]✉ and Jin Liu[1]✉

Abstract

The emerging hybrid integrated quantum photonics combines the advantages of different functional components into a single chip to meet the stringent requirements for quantum information processing. Despite the tremendous progress in hybrid integrations of III-V quantum emitters with silicon-based photonic circuits and superconducting single-photon detectors, on-chip optical excitations of quantum emitters via miniaturized lasers towards single-photon sources (SPSs) with low power consumptions, small device footprints, and excellent coherence properties is highly desirable yet illusive. In this work, we present realizations of bright semiconductor SPSs heterogeneously integrated with on-chip electrically-injected microlasers. Different from previous one-by-one transfer printing technique implemented in hybrid quantum dot (QD) photonic devices, multiple deterministically coupled QD-circular Bragg Grating (CBG) SPSs were integrated with electrically-injected micropillar lasers at one time via a potentially scalable transfer printing process assisted by the wide-field photoluminescence (PL) imaging technique. Optically pumped by electrically-injected microlasers, pure single photons are generated with a high-brightness of a count rate of 3.8 M/s and an extraction efficiency of 25.44%. Such a high-brightness is due to the enhancement by the cavity mode of the CBG, which is confirmed by a Purcell factor of 2.5. Our work provides a powerful tool for advancing hybrid integrated quantum photonics in general and boosts the developments for realizing highly-compact, energy-efficient and coherent SPSs in particular.

Introduction

Photonic quantum technology harnessing the superposition and entanglement of non-classical states of light has enabled secure communication, superfast computation, and accurate metrology[1]. Introductions of integrated optics to modern quantum photonics facilitate the abilities of generations, manipulations, and detections of quantum states of light by using more than 1000 programable components on a phase-stable chip with a millimeter-scale footprint[2]. Similar to conventional integrated optics, it is not realistic for a single material platform to satisfy all the functionalities required for each distinct component in quantum information processing tasks[3,4]. For example, III–V semiconductor QD SPSs so far have exhibited the best performances in terms of simultaneous high-degrees of source brightness, single-photon purity, and photon indistinguishability[5–10] while silicon photonic circuits excel in reconfigurable manipulations of multi-photon[11,12] or high-dimensional quantum states[13,14] with high operational fidelities. Thus, hybrid integrated quantum photonic circuits are currently being under extensive explorations worldwidely by heterogeneously integrating III-V solid-state quantum

Correspondence: Zhichuan Niu (zcniu@semi.ac.cn) or
You-ling Chen (ylchen@semi.ac.cn) or Jin Liu (liujin23@mail.sysu.edu.cn)
[1]State Key Laboratory of Optoelectronic Materials and Technologies, School of Physics, School of Electronics and Information Technology, Sun Yat-sen University, 510275 Guangzhou, China
[2]Hisilicon Research, Huawei Technologies Co., Ltd, 518129 Shenzhen, China
Full list of author information is available at the end of the article
These authors contributed equally: Xueshi Li, Shunfa Liu.

emitters as deterministic quantum light sources with silicon-based photonic circuits[15–18] and superconducting single-photon detectors[19–21] on a single chip. Despite remarkable progress in the development of the heterogeneously integrated photonic components, there remains a large performance gap between the fully-fledged integrated quantum photonic devices and their classical photonic counterparts—that is—chip-integrated pumping lasers. The on-chip optical excitation of solid-state quantum emitters by using microlasers results in much lower power consumptions, significantly reduced device footprints, and potentially ideal coherence properties of the emitted photons. In a conventional off-chip optical excitation scheme, radiations from bulky and high-power lasers have to be greatly attenuated to a few tens of nano-Watt for creating carriers in QDs, in which most of the radiation power of the bulky external lasers is wasted. In addition, optical pumping schemes, especially resonant[22], quasi-resonant[23], two-photon resonant[24–26], and phonon-assisted excitation[27], are able to deliver highly-coherent single photons with a near-unity photon indistinguishability, appreciably surpassing the record value of 41% achieved under the electrical injection condition[28].

Moving towards integrations of QD SPSs and microlasers, electrically-injected micropillars have been successfully demonstrated to excite QD SPSs in an off-chip manner[29]. The on-chip excitations of QDs have also been demonstrated in a monolithic chip with unsatisfactory source brightnesses. In monolithic platforms, both SPSs and microlasers are limited to the same geometry, e.g., micropillars[30,31] or planar cavities[32], which prevents the independent optimizations of each component. To better separate optimizations of laser excitations and single-photon emissions, we combine, in this work, deterministically-fabricated planar CBGs as bright SPSs and electrically-injected micropillars as highly-directional microlasers on a single chip. These two components are individually optimized and heterogeneously integrated together by using a potentially scalable transfer printing process capable of fabricating a multitude of devices in a single run. The single QD was pumped by an on-chip micropillar laser under electrical injections, exhibiting high-performances in terms of the source brightness and single-photon purity thanks to the coupling of the QD to the cavity mode of the CBG. This work constitutes a major step in developing highly-efficient and coherent semiconductor SPSs with small footprints for hybrid integrated quantum photonics.

Results

Figure 1 presents the building blocks and the concept of our device. A suspended GaAs CBG with a single QD embedded in the center serves as an efficient SPS, as shown in Fig. 1a. The CBG consists of a GaAs microdisk surrounded by a serial of shallowly etched air trenches. Photons emitted from the QD in the center of CBG are mostly confined in the suspended membrane. Due to the presence of second-order Bragg gratings, parts of the emitted photons from the QD are scattered upwards for efficient collections and the others are reflected back to form a cavity for enhancing the strength of light-matter interactions[33–38]. To optically pump the QD-CBG SPS, we explore electrically-injected micropillar lasers[39] consisting of quantum wells sandwiched between two distributed Bragg Reflectors (DBRs), as schematically shown in Fig. 1b. These two elements are assembled in a way that the CBG

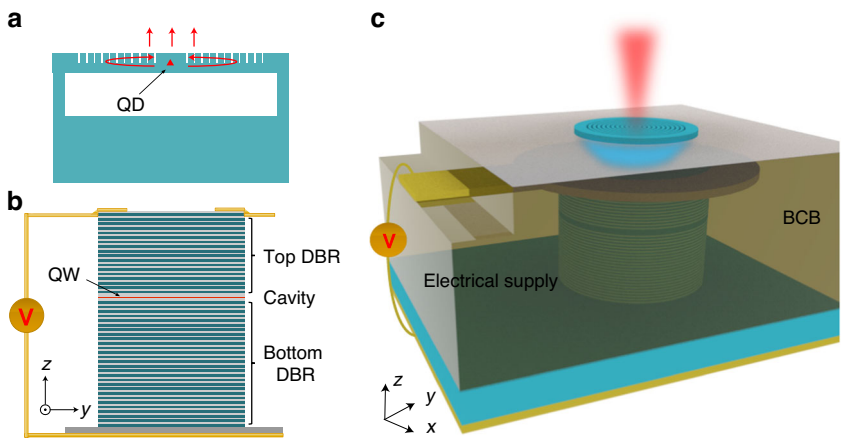

Fig. 1 Illustration of the hybrid integrated SPS. a CBG with a single QD embedded for bright single-photon emissions. The single photons emitted from the QD are confined in the suspended membrane by total internal reflections, partially reflected to the center of the CBG and partially scattered to the top by second-order Bragg gratings consisting of shallowly etched air trenches. **b** Micropillars with embedded quantum wells for electrically-injected microlasers. **c** Illustration of the hybrid integrated device. Pumped by the on-chip micropillar laser with electrical injections, the QD in the CBG emits highly-directional single photons to the free space

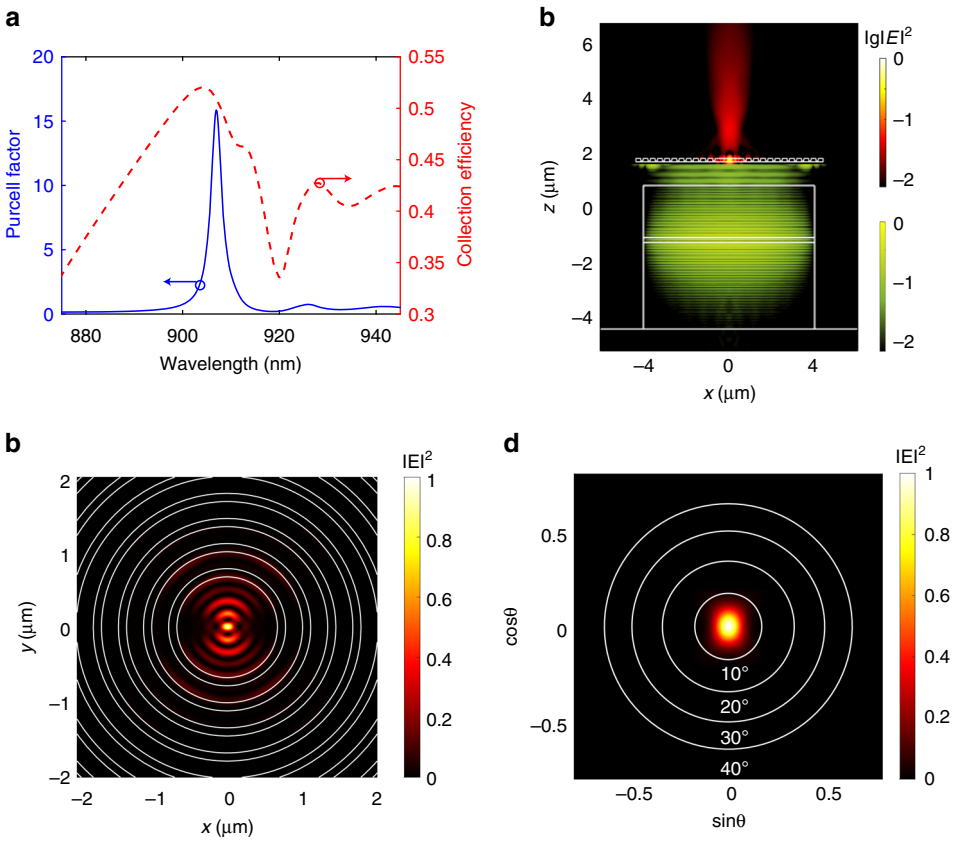

Fig. 2 Numerical simulations of the device. a Purcell factor and extraction efficiency of the hybrid integrated SPS. A numerical aperture (NA) of 0.65 was used in the extraction efficiency calculation. **b** The near-field intensity distribution of the cavity mode of the CBG shows highly-localized electromagnetic fields. **c** The beam propagations of laser emissions from the micropillar and the single-photon emissions from the CBG in the XZ plane. The QD is efficiently excited by the micropillar laser and emits highly-directional single photons. **d** The far-field intensity distribution of single-photon emissions exhibits a divergent angle within 10°

is located right on top of the micropillar laser and an additional spacer is designed specifically to separate cavity modes in each distinct component, as schematically shown in Fig. 1c. Optically driven by the coherent photons emitted from the electrically-injected micropillar laser, the QD in the CBG emits highly-directional single photons upwards to the collection optics.

With the above device design, we further explore the optical performance of a single-QD in the hybrid cavities by modeling the extraction efficiency and the Purcell factor, as shown in Fig. 2a. The extraction efficiency is defined as the fraction of the photons collected by the objective over all the photons emitted by the QD. The cavity effect of the CBG is revealed by a Lorentzian shape of the Purcell factor with a maximal value of ~15 and a full width at half maximum of ~3 nm, corresponding to a Q-factor of ~303. The bandwidth for efficient collections of the single photons are much broader, showing extraction efficiencies >40% over 33 nm. Such an appreciable Purcell factor is due to the tight light confinement of the CBG cavity mode, as presented in Fig. 2b. We chose a 2 μm gap filled with benzocyclobutene (BCB) between the CBG and the micropillar laser so that the cavity mode of the CBG is not perturbed by the presence of the micropillar. The excitation of the QD by the micropillar laser (blue) and the highly-directional single-photon emissions (red) can be clearly identified from the beam propagation profiles in the XZ plane of the device, as shown in Fig. 2c. Figure 2d further shows the far-field pattern of single-photon emissions from the CBG device, exhibiting a divergent angle within 10° for the efficient collection.

We take advantage of the well-developed transfer printing technique which has been successfully demonstrated for building hybrid quantum photonic devices[17,18,40]. However, the implementations of such a technique to QD devices so far are limited in a one-by-one fashion due to the intrinsic random nature in QD's spatial position. In order to obtain multiple devices with high yields at one time, we utilized the wide-field PL imaging technique to deterministically fabricate coupled CBG-QD devices[34,41,42]. In such a process, metallic

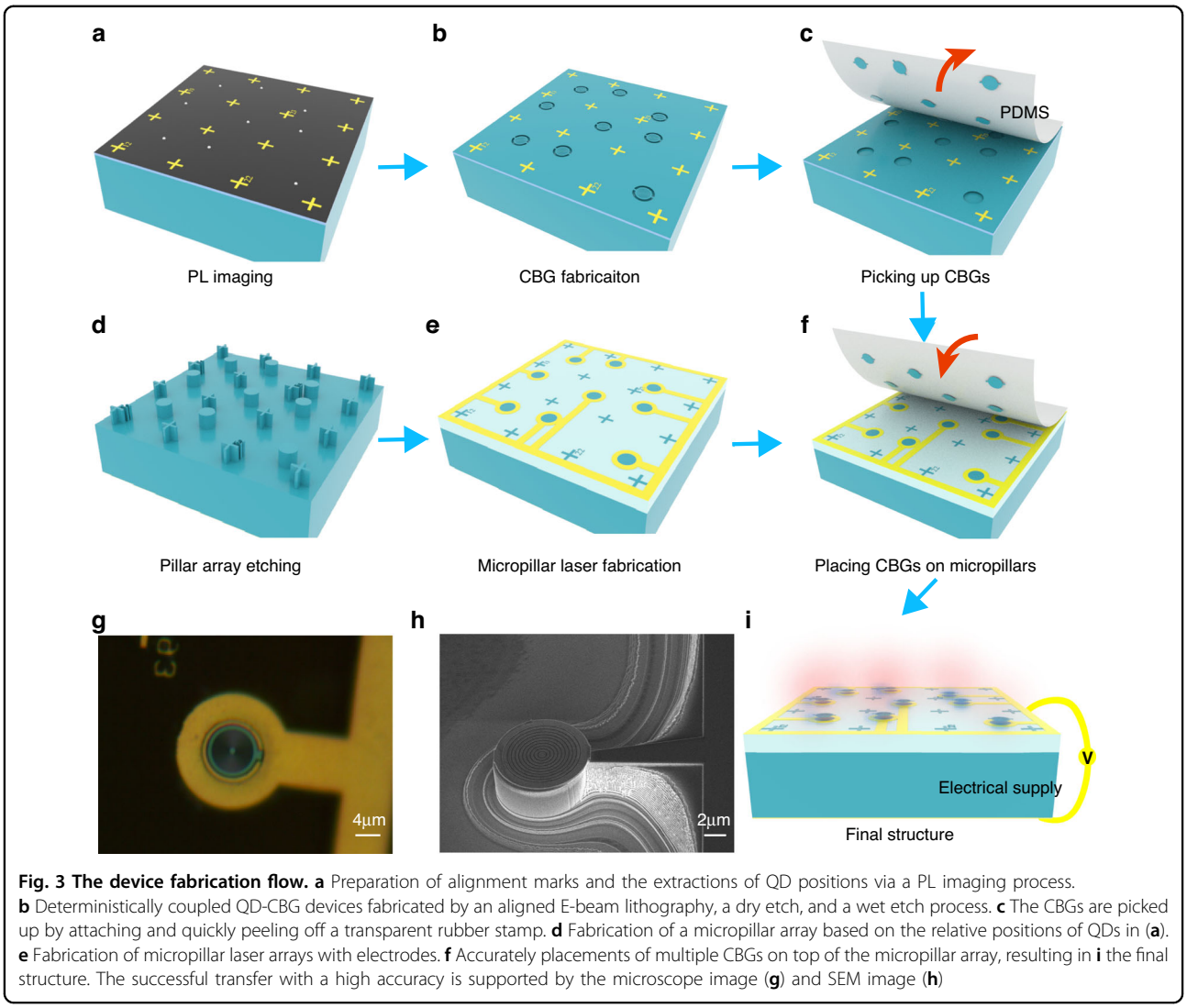

Fig. 3 The device fabrication flow. a Preparation of alignment marks and the extractions of QD positions via a PL imaging process. **b** Deterministically coupled QD-CBG devices fabricated by an aligned E-beam lithography, a dry etch, and a wet etch process. **c** The CBGs are picked up by attaching and quickly peeling off a transparent rubber stamp. **d** Fabrication of a micropillar array based on the relative positions of QDs in (**a**). **e** Fabrication of micropillar laser arrays with electrodes. **f** Accurately placements of multiple CBGs on top of the micropillar array, resulting in **i** the final structure. The successful transfer with a high accuracy is supported by the microscope image (**g**) and SEM image (**h**)

alignment marks were firstly prepared on an III-V QD wafer and then the spatial positions of individual QDs respective to the alignment marks were extracted from PL images, as shown in Fig. 3a. The deterministically coupled QD SPSs were then obtained by an aligned E-beam lithography, a chloride-based dry etch and a selective wet etch, as presented in Fig. 3b. Then, we used transfer printing to pick up multiple processed CBGs from the substrate using a transparent rubber stamp, as schematically shown in Fig. 3c. On the other III–V wafer containing quantum wells and DBRs, electrically-injected microlasers were fabricated in a specific array based on the relative positions of fabricated CBGs, with the similar processing recipe for micropillar SPSs[24,43], as shown in Fig. 3d, e. The micropillar array was covered with a ~2 μm thick BCB spacer between the microlaser and SPS in order to maintain the cavity modes of the on-substrate CBGs. Because the cavity mode slightly leaks out of the thin membrane in z direction, as shown in Fig. S(5), direct placements of CBGs on tops of micropillars result in the vanish of CBG modes, significantly reducing the brightness of the SPSs. We then aligned multiple CBGs to the micropillar laser array under an optical microscope and released the CBGs on micropillars by slowly and gently peeling the stamp off, as shown in Fig. 3f. A schematic of the completed hybrid integrated SPS array is shown in Fig. 3i, in which multiple QDs coupled to CBGs can be simultaneously pumped by the underneath electrically-injected micropillar laser array. In a representative microscope image of the transferred device, a CBG can be clearly identified in the center of the micropillar laser, as presented in Fig. 3g. The successful transfer printing with a high alignment accuracy was further supported by a scanning electron microscope (SEM) image of a test device without planarizing the micropillar laser using BCB, as presented in Fig. 3h.

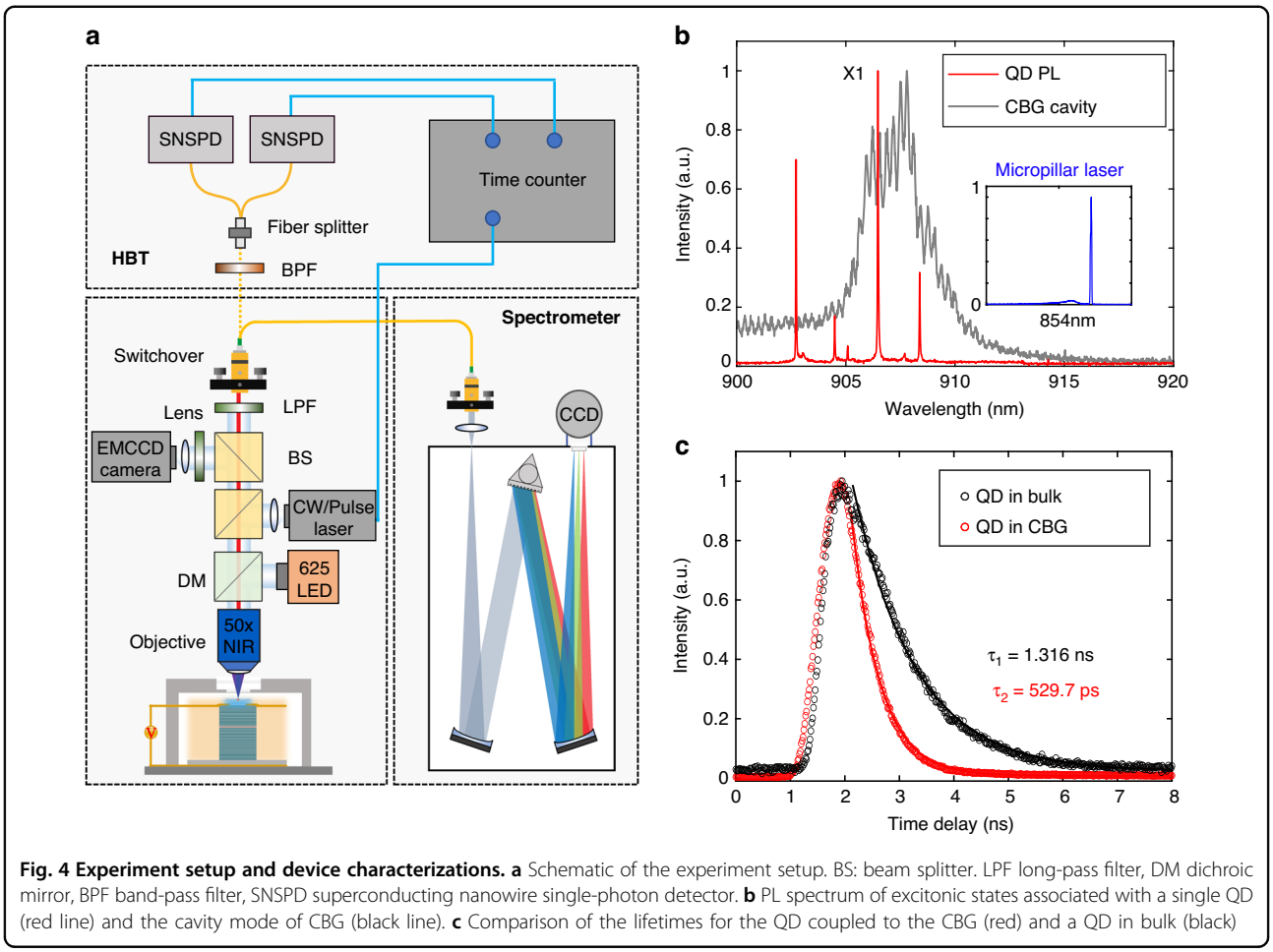

Fig. 4 Experiment setup and device characterizations. a Schematic of the experiment setup. BS: beam splitter. LPF long-pass filter, DM dichroic mirror, BPF band-pass filter, SNSPD superconducting nanowire single-photon detector. **b** PL spectrum of excitonic states associated with a single QD (red line) and the cavity mode of CBG (black line). **c** Comparison of the lifetimes for the QD coupled to the CBG (red) and a QD in bulk (black)

The optical setup and the device characterizations are shown in Fig. 4. The hybrid integrated devices are placed on three-dimensional nanopositioners located in a closed circle cryostat with a base temperature of 5.4 K. The QD SPSs can be either excited by the on-chip micropillar lasers or by external continuous wave (CW) and pulsed lasers via a × 50 objective with a numerical aperture of 0.65. The emitted single photons are collected by the same objective and sent to a monochromator for the spectral analysis or to single-photon detectors for lifetime characterizations and Hanbury-Brown-Twiss (HBT) measurements, as shown in Fig. 4a. By applying a small bias voltage to the micropillar laser, sharp excitonic lines (red) from the single QD are identified in the μPL spectrum, as presented in Fig. 4b. The bright exciton (X1) is spectrally close to the cavity mode (black) of the CBG. The emission spectrum of the electrically-injected micropillar laser is shown in the inset of Fig. 4b, featuring a sharp lasing peak at 854 nm. Such near-infrared micropillar lasers are compatible with industry-standard, which renders practical application of our hybrid QDs SPS-Micropillar laser device convenient. The coupling between the QD and the CBG was revealed by the shortened lifetime of X1. A lifetime of 529 ps for QD in the CBG was extracted, corresponding to a Purcell factor of 2.5 compared to a lifetime of 1316 ps for the QD in bulk. The large deviation of the simulated Purcell factor from the experimental result is a combination of the non-ideal QD position and the long carrier relaxation time under above-band excitation[44].

A single-photon purity $g^{(2)}(0)$ as low as 0.03 ± 0.01 (deconvoluted with the detector response[15]) under on-chip excitation condition was extracted from the second-order correlation measurement in an HBT interferometer, see Fig. 5a. As a comparison, we used an external CW diode laser at 854 nm to excite the QD and obtained a very similar $g^{(2)}(0)$ of 0.02 ± 0.01, as shown in Fig. 5b, which suggests that the on-chip optical excitation by integrated lasers can deliver the same performance as that obtained under the widely-used external optical pumping. The photon count rate and $g^{(2)}(0)$ as a function of the bias voltage are shown in Fig. 5c. Both photon flux and $g^{(2)}(0)$ increase[45–47] with the rise of the applied bias voltage and the maximal count rate (not saturated) up to 3.8 M/s with

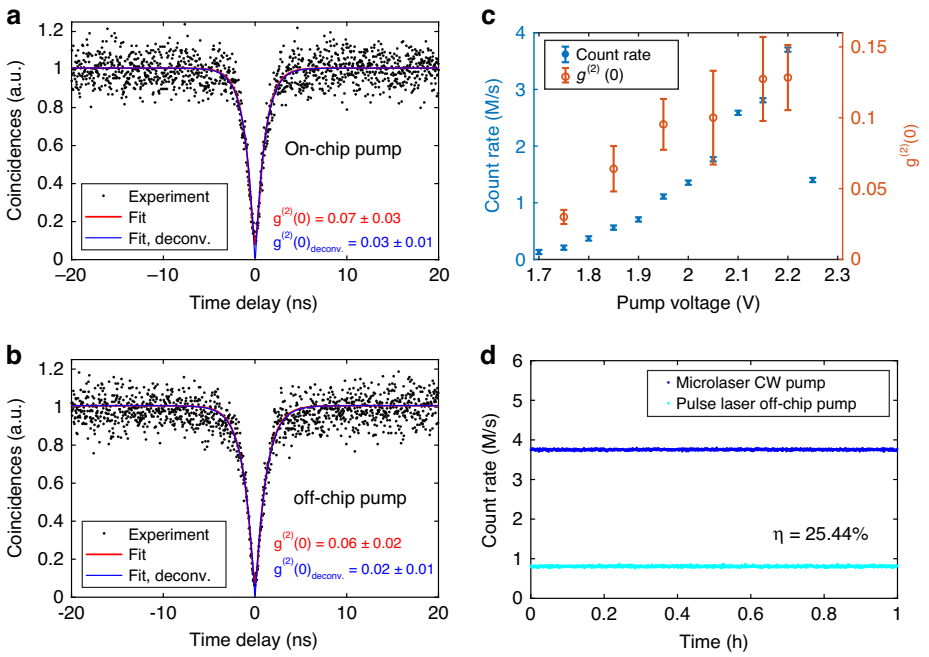

Fig. 5 Source brightness and single-photon purity. a, **b** Second-order correlation as a function of time delay for the QD pumped by the on-chip microlaser and an external CW laser diode. Black dots mark experimental data. The red and blue curves are the fits with and without deconvolutions of the detector response, respectively. **c** Photon count rate (blue circles) and $g^{(2)}(0)$ (brown circles) as a function of the bias voltage applied to the micropillar laser. **d** Saturation count rates from X1 pumped by the micropillar laser (dark blue) operating in a CW mode and a fs pulsed laser (bright blue)

a $g^{(2)}(0)$ of 0.13 ± 0.02 was obtained under the voltage of 2.2 V. Further increase of the bias voltage results in a rapid quenching of single-photon emissions, which is probably due to the detrimental thermal effect associated with the BCB spacer. We further quantified the extraction efficiency of the hybrid integrated SPS by externally exciting the device using a femto-second (fs) pulsed laser with a repetition rate of 79.6 MHz. The saturated count rate under pulsed excitation (see Fig. S10) together with the count rate under on-chip CW pumping are presented in Fig. 5d. The generated photon rate is monitored continuously over 1 h to check the long-term operational stability of the device. Under the pulsed excitation, each laser pulse is presumably to generate one single photon[48]. By measuring the count rate in the single-photon detector and carefully calibrating the system detection efficiency (see details in SI), an extraction efficiency of 25.44% was obtained for the hybrid integrated SPSs.

Discussion

To conclude, we have demonstrated hybrid integrations of bright SPSs with on-chip electrically-injected micropillar lasers. Assisted by the QD PL imaging technique, our optimized transfer printing process operates at a multi-device level, showing potential scalability for hybrid integrated quantum photonics. The single QD in the CBG was optically pumped by an on-chip micropillar laser, exhibiting a CW photon count rate of 3.8 M/s with $g^{(2)}(0)$ of 0.13 ± 0.02 under a high bias voltage and a very low $g^{(2)}(0)$ of 0.03 ± 0.01 under a low bias voltage. Our device experienced a Purcell factor of 2.5 and an extraction efficiency of 25.44% thanks to the coupling of QD to the CBG cavity mode. This work serves as a crucial step towards energy-saving on-chip single-photon and entangled pair sources for hybrid integrated quantum photonics[49]. Our devices could be simultaneously coupled to an optical fiber array to realize the plug-and-play function, which has broad application prospects in quantum key distribution. Moving forwards, on-chip resonant excitations (see a realistic proposal in SI) by spectrally tuning the microlaser wavelength to the QD transition energies could be pursued to further improve the photon indistinguishability for advancing photonic quantum technologies.

Materials and methods

Epitaxial growth of QDs

The samples were grown using solid source molecular beam epitaxy on semi-insulating GaAs (001) substrates. After deoxidization at a temperature of 680 °C for 10 minutes and growth of 300 nm GaAs buffer layer at 660 °C, a 1000 nm $Al_{0.8}Ga_{0.2}As$ sacrificial layer was grown

at 620 °C. The InAs QDs were embedded in the middle of a GaAs layer with a thickness of 160 nm. The InAs QDs were deposited at the temperature of (Tc-27) °C with an indium flux rate of 0.004 ML/s and an As flux pressure of 5×10^{-7} Torr. The deposition temperatures are calibrated by the transition temperature Tc when the surface reconstruction pattern of GaAs in high-energy electron diffraction (RHEED) transfers from (2 × 4) to (2 × 3). Then the InAs QDs were capped with a thin layer of 0.3 nm AlAs and 6.5 nm GaAs, followed by a 200 s indium flushing step at 660 °C.

Fabrication of the coupled QD-CBG

The process starts with the III-V wafer consists of a 160-nm-thin GaAs membrane containing InAs quantum dots (QDs) grown on top of a sacrificial layer (1 μm $Al_{0.8}Ga_{0.2}As$) and a GaAs substrate. To acquire the positions of QDs, firstly, metallic alignment marks are created on the surface of the sample with standard E-beam lithography, metal deposition, and lift-off processes. Then, the positions of the QDs respective to the alignment marks are extracted from the wide-field PL images. The PL imaging process has an accuracy of about 20 nm[8]. After that, the shallow etched CBGs with QD in the center are fabricated through another aligned E-beam lithography followed by a chlorine-based dry etch process. After removing the photoresist by oxygen plasma surface treatments, we dip the sample in the acid solution of HF 10% for the necessary time to remove the sacrificial layer. We finally obtain the suspended deterministically coupled QD-CBG devices by drying the sample in isopropanol. The detailed fabrication flow of the coupled QD-CBG devices is presented in Supplementary Fig. S1.

Fabrication of the micropillar laser

The wafer consists of a single layer GaAs with QW between 23(30) top(bottom) $GaAs/Al_{0.9}Ga_{0.1}As$ distributed Bragg reflector (DBRs) provided by EPIHOUSE. In order to achieve an electrically pumped micropillar laser, we need to properly dop the wafers. The epitaxial n-type and p-type regions are realized by doping the GaAs during the growth with silicon and carbon, respectively. The first step in creating the micropillar laser is the fabrication of electrical contacts to the n-doped layers. We obtain the Ni/Ge/Au/Ni/Au contacts on the back of the wafer by E-beam evaporation, followed by an annealing process. Then, the masks of the electrically-injected micropillar lasers and alignment marks are fabricated in a specific array based on the relative positions of fabricated CBGs by using an E-beam lithography. After the chlorine-based dry etch process, we use BCB to flatten the micropillars to ensure that the upper surfaces of the micropillars are just exposed. This process requires multiple spin-coatings of the photoresist, annealing, and dry etching processes. Finally, the positive electrode is created by using an E-beam lithography, metal evaporation, and lift-off processes. The detailed fabrication flow of the micropillar laser is presented in Supplementary Fig. S2.

Transfer printing process

After the fabrications of the CBGs, we realize the micropillars at the corresponding positions according to the layout of the CBG array. Therefore, during the transfer process, we can align multiple CBGs with micropillars to achieve potentially scalable device integrations. We show 20 of 26 transferred devices at one time in Supplementary Fig. S5.

Acknowledgements

This research was supported by National Natural Science Foundation of China (62035017, 12074442); National Key Research and Development Program of China (2018YFA0306103); Science and Technology Program of Guangzhou (202103030001); Hisilicon Technologies CO., LIMITED and the national supercomputer center in Guangzhou.

Author details

[1]State Key Laboratory of Optoelectronic Materials and Technologies, School of Physics, School of Electronics and Information Technology, Sun Yat-sen University, 510275 Guangzhou, China. [2]Hisilicon Research, Huawei Technologies Co., Ltd, 518129 Shenzhen, China. [3]State Key Laboratory for Superlattice and Microstructures, State Key Laboratory on Integrated Optoelectronics, Institute of Semiconductors, Chinese Academy of Sciences, 100083 Beijing, China. [4]Center of Materials Science and Optoelectronics Engineering, University of Chinese Academy of Sciences, 100049 Beijing, China

Author contributions

Y.C. and J.L. conceived the project. X.L., R.S., and S.L. performed numerical simulations. C.S., Y.Y., H.N., H.L., X.S., and Z.N. grew the wafers. X.L., J.M., and S.L. performed optical characterizations. X.L., W.G., S.L., and J.L. analyzed the data. J.L. wrote the manuscript with inputs from all authors. Z.N., Y.C., and J.L. supervised the project.

Conflict of interest

The authors declare no competing interests.

Supplementary information The online version contains supplementary material available at https://doi.org/10.1038/s41377-023-01110-9.

Received: 16 November 2022 Revised: 7 February 2023 Accepted: 16 February 2023
Published online: 06 March 2023

References

1. O'Brien, J. L., Furusawa, A. & Vučković, J. Photonic quantum technologies. *Nat. Photon.* **3**, 687–695 (2009).
2. Wang, J. W. et al. Integrated photonic quantum technologies. *Nat. Photon.* **14**, 273–284 (2020).
3. Elshaari, A. W. et al. Hybrid integrated quantum photonic circuits. *Nat. Photon.* **14**, 285–298 (2020).
4. Kim, J. H. et al. Hybrid integration methods for on-chip quantum photonics. *Optica* **7**, 291–308 (2020).
5. Senellart, P., Solomon, G. & White, A. High-performance semiconductor quantum-dot single-photon sources. *Nat. Nanotechnol.* **12**, 1026–1039 (2017).
6. Wang, H. et al. Towards optimal single-photon sources from polarized microcavities. *Nat. Photon.* **13**, 770–775 (2019).
7. Tomm, N. et al. A bright and fast source of coherent single photons. *Nat. Nanotechnol.* **16**, 399–403 (2021).

8. He, Y. M. et al. Deterministic implementation of a bright, on-demand single-photon source with near-unity indistinguishability via quantum dot imaging. *Optica* **4**, 802–808 (2017).
9. Uppu, R. et al. Scalable integrated single-photon source. *Sci. Adv.* **6**, eabc8268 (2020).
10. Zhou, X., Zhai, L. & Liu, J. Epitaxial quantum dots: a semiconductor launchpad for photonic quantum technologies. *Photon. Insights* **1**, R07 (2023).
11. Qiang, X. G. et al. Large-scale silicon quantum photonics implementing arbitrary two-qubit processing. *Nat. Photon.* **12**, 534–539 (2018).
12. Li, L. et al. Metalens-array–based high-dimensional and multiphoton quantum source. *Science* **368**, 1487–1490 (2020).
13. Wang, J. W. et al. Multidimensional quantum entanglement with large-scale integrated optics. *Science* **360**, 285–291 (2018).
14. Zhang, M. et al. Generation of multiphoton quantum states on silicon. *Light Sci. Appl.* **8**, 41 (2019).
15. Davanco, M. et al. Heterogeneous integration for on-chip quantum photonic circuits with single quantum dot devices. *Nat. Commun.* **8**, 889 (2017).
16. Zadeh, I. E. et al. Deterministic integration of single photon sources in silicon based photonic circuits. *Nano Lett.* **16**, 2289–2294 (2016).
17. Katsumi, R. et al. Quantum-dot single-photon source on a CMOS silicon photonic chip integrated using transfer printing. *APL Photon.* **4**, 036105 (2019).
18. Katsumi, R. et al. Transfer-printed single-photon sources coupled to wire waveguides. *Optica* **5**, 691–694 (2018).
19. Schwartz, M. et al. Fully on-chip single-photon hanbury-brown and twiss experiment on a monolithic semiconductor–superconductor platform. *Nano Lett.* **18**, 6892–6897 (2018).
20. Najafi, F. et al. On-chip detection of non-classical light by scalable integration of single-photon detectors. *Nat. Commun.* **6**, 5873 (2015).
21. Reithmaier, G. et al. On-chip time resolved detection of quantum dot emission using integrated superconducting single photon detectors. *Sci. Rep.* **3**, 1901 (2013).
22. He, Y. M. et al. On-demand semiconductor single-photon source with near-unity indistinguishability. *Nat. Nanotechnol.* **8**, 213–217 (2013).
23. Gschrey, M. et al. Highly indistinguishable photons from deterministic quantum-dot microlenses utilizing three-dimensional in situ electron-beam lithography. *Nat. Commun.* **6**, 7662 (2015).
24. Wei, Y. M. et al. Tailoring solid-state single-photon sources with stimulated emissions. *Nat. Nanotechnol.* **17**, 470–476 (2022).
25. Jayakumar, H. et al. Deterministic photon pairs and coherent optical control of a single quantum dot. *Phys. Rev. Lett.* **110**, 135505 (2013).
26. Reindl, M. et al. Phonon-assisted two-photon interference from remote quantum emitters. *Nano Lett.* **17**, 4090–4095 (2017).
27. Thomas, S. E. et al. Bright polarized single-photon source based on a linear dipole. *Phys. Rev. Lett.* **126**, 233601 (2021).
28. Schlehahn, A. et al. An electrically driven cavity-enhanced source of indistinguishable photons with 61% overall efficiency. *APL Photon.* **1**, 011301 (2016).
29. Kreinberg, S. et al. Quantum-optical spectroscopy of a two-level system using an electrically driven micropillar laser as a resonant excitation source. *Light Sci. Appl.* **7**, 41 (2018).
30. Munnelly, P. et al. Electrically tunable single-photon source triggered by a monolithically integrated quantum dot microlaser. *ACS Photon.* **4**, 790–794 (2017).
31. Stock, E. et al. On-chip quantum optics with quantum dot microcavities. *Adv. Mater.* **25**, 707–710 (2013).
32. Lee, J. P. et al. Electrically driven and electrically tunable quantum light sources. *Appl. Phys. Lett.* **110**, 071102 (2017).
33. Davanço, M. et al. A circular dielectric grating for vertical extraction of single quantum dot emission. *Appl. Phys. Lett.* **99**, 041102 (2011).
34. Sapienza, L. et al. Nanoscale optical positioning of single quantum dots for bright and pure single-photon emission. *Nat. Commun.* **6**, 7833 (2015).
35. Wang, H. et al. On-demand semiconductor source of entangled photons which simultaneously has high fidelity, efficiency, and indistinguishability. *Phys. Rev. Lett.* **122**, 113602 (2019).
36. Abudayyeh, H. et al. Single photon sources with near unity collection efficiencies by deterministic placement of quantum dots in nanoantennas. *APL Photon.* **6**, 036109 (2021).
37. Abudayyeh, H. et al. Overcoming the rate-directionality trade-off: a room-temperature ultrabright quantum light source. *ACS Nano* **15**, 17384–17391 (2021).
38. Nikolay, N. et al. Accurate placement of single nanoparticles on opaque conductive structures. *Appl. Phys. Lett.* **113**, 113107 (2018).
39. Gies, C. & Reitzenstein, S. Quantum dot micropillar lasers. *Semicond. Sci. Technol.* **34**, 073001 (2019).
40. Jin, T. T. et al. Generation of polarization-entangled photons from self-assembled quantum dots in a hybrid quantum photonic chip. *Nano Lett.* **22**, 586–593 (2022).
41. Liu, J. et al. Cryogenic photoluminescence imaging system for nanoscale positioning of single quantum emitters. *Rev. Sci. Instrum.* **88**, 023116 (2017).
42. Liu, S. F., Srinivasan, K. & Liu, J. Nanoscale positioning approaches for integrating single solid-state quantum emitters with photonic nanostructures. *Laser Photon. Rev.* **15**, 2100223 (2021).
43. Liu, S. F. et al. Dual-resonance enhanced quantum light-matter interactions in deterministically coupled quantum-dot-micropillars. *Light Sci. Appl.* **10**, 158 (2021).
44. Liu, F. et al. High Purcell factor generation of indistinguishable on-chip single photons. *Nat. Nanotechnol.* **13**, 835–840 (2018).
45. Madsen, K. H. et al. Efficient out-coupling of high-purity single photons from a coherent quantum dot in a photonic-crystal cavity. *Phys. Rev. B* **90**, 155303 (2014).
46. Kolatschek, S. et al. Bright Purcell enhanced single-photon source in the telecom o-band based on a quantum dot in a circular Bragg grating. *Nano Lett.* **21**, 7740–7745 (2021).
47. Xu, S. W. et al. Bright single-photon sources in the telecom band by deterministically coupling single quantum dots to a hybrid circular Bragg resonator. *Photon. Res.* **10**, B1–B6 (2022).
48. Lodahl, P., Mahmoodian, S. & Stobbe, S. Interfacing single photons and single quantum dots with photonic nanostructures. *Rev. Mod. Phys.* **87**, 347–400 (2015).
49. Liu, J. et al. Emerging material platforms for integrated microcavity photonics. *Sci. China Phys. Mech. Astron.* **65**, 104201 (2022).